Temperature-Dependent Photophysical, Photochemical and Redox Properties of Novel Complexes $(CO)_2CpRu–Ru(L_n)–RuCp(CO)_2$ and $(CO)_2CpRu–Ru(L_n)–SnPh_3$ [L_n = $(CO)_2$(*N,N′*-diisopropyl-1,4-diaza-1,3-butadiene)]

Joris van Slageren,[a] František Hartl,*[a] and Derk J. Stufkens[a]

Keywords: Photochemistry / Electrochemistry / Ruthenium compounds / α-Diimine complexes

The photophysical, photochemical and redox properties of the title complexes were investigated. Resonance Raman measurements revealed the lowest-energy electronic transition to possess σ→π* character. At low temperatures, long-lived near-IR emission was observed. Irradiation in solution results in homolytic splitting of a Ru–Ru bond as the primary step, followed by secondary reactions of the radical fragments depending on the experimental conditions. (Spectro)-electrochemical investigations of the title species proved that the axial [$RuCp(CO)_2$] groups exert a stabilising influence on the corresponding radical cations, while destabilising the corresponding radical anions, compared to the redox behaviour of other ruthenium complexes of this type.

Introduction

The photochemical, photophysical and redox properties of the complexes *trans,cis*-[$Ru(L^1)(L^2)(CO)_2$(*i*-Pr–DAB)] (*i*-Pr–DAB = *N,N′*-diisopropyl-1,4-diaza-1,3-butadiene) have been studied extensively in our laboratory.[1–5] In this general formula L^1 and L^2 represent electron donating ligands such as alkyl or metal-containing groups. It was shown that in the lowest excited state of these complexes electron density was transferred from the L^1–Ru–L^2 σ system to the π* orbital of *i*-Pr–DAB, which contrasts with the lowest MLCT state of [$Ru(Cl)(Me)(CO)_2$(*i*-Pr–DAB)] and the XLCT (X = I) state of [$Ru(I)(Me)(CO)_2$(*i*-Pr–DAB)].[6–8] One of the consequences of this σπ* or Sigma-Bond-to-Ligand Charge Transfer (SBLCT) excited state character is a dramatic increase in excited state lifetime.[2] On the other hand, since the L^1–Ru–L^2 σ orbital is high in energy (and hence the corresponding σ* orbital lies relatively low) the dissociative σσ* state is thermally accessible. This imparts all members of the series [$Ru(L^1)(L^2)(CO)_2$(*i*-Pr–DAB)] with a certain degree of photoreactivity.

The present study was undertaken to investigate the influence of strongly electron releasing axial ligands on photophysical and photochemical behaviour. Two novel complexes bearing one or two [$RuCp(CO)_2$] groups as axial ligands were therefore synthesized. It was expected that incorporation of these ligands would shift the electronic absorption maximum to lower energy, hence giving rise to near-infrared emission. This is very interesting in view of the challenging application of such compounds as luminescent labels e.g. in biochemical separations, since background luminescence is negligible in the near infrared spectral region. A long luminescence lifetime is also desirable in order to make time-gated detection viable. In order to understand the influence of the electron releasing [$RuCp(CO)_2$] axial ligand(s) on the electronic properties and reactivity of the title complexes in more detail, a (spectro)electrochemical study was also undertaken.

[a] Institute of Molecular Chemistry,
Universiteit van Amsterdam
Nieuwe Achtergracht 166, NL-1018 WV Amsterdam,
The Netherlands
E-mail: hartl@anorg.chem.uva.nl

Results and Discussion

Spectroscopic Properties

The novel title compounds, purple [$Ru(SnPh_3)\{RuCp(CO)_2\}(CO)_2$(*i*-Pr–DAB)] (**1**) and green [$Ru\{RuCp(CO)_2\}_2(CO)_2$(*i*-Pr–DAB)] (**2**) were prepared by addition of $K[RuCp(CO)_2]$ to [$Ru(Cl)(SnPh_3)(CO)_2$(*i*-Pr–DAB)] and [$RuI_2(CO)_2$(*i*-Pr–DAB)], respectively, according to the procedure used for the synthesis of [$Ru\{Re(CO)_5\}_2(CO)_2$(*i*-Pr–DAB)].[9] Both complexes are highly photoreactive in solution, but virtually photostable in the solid state. The ^1H and ^{13}C NMR chemical shifts for the coordinated *i*-Pr–DAB ligand are similar to those found for other *trans,cis*-[$Ru(L^1)(L^2)(CO)_2$(*i*-Pr–DAB)] complexes, pointing to axial positions of the [$RuCp(CO)_2$] groups (See Figure 1). Both **1** and **2** may exist as a mixture of several rotamers in solution.

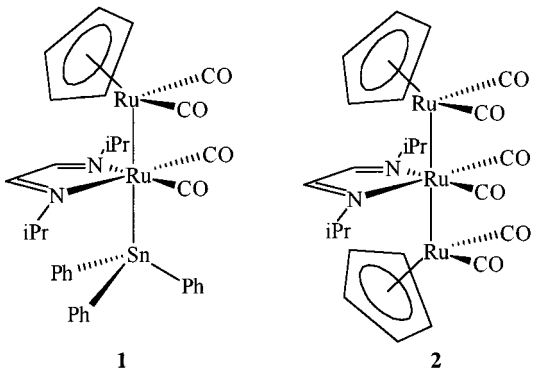

Figure 1. Schematic molecular structures of the complexes **1** and **2**

  1434–1948/00/0505–0847 $ 17.50+.50/0

Table 1. Spectroscopic data for complexes **1** and **2**

	UV/Vis[a] λ_{max}[b] (ε[c])	Δ[d]	IR[e]	Resonance Raman (cm^{-1})
1	571 (5770), 383, 333, 306	368	1993m, 1960s, 1933s, 1918w	1460s, 1281s, 951s, 829s, 609m, 416w, 242m, 192m
2	605 (7070), 463, 352	82	1991w, 1967s, 1946s, 1926s, 1919sh, 1897w	1459vw, 1281vw, 954m, 833m, 601m, 499w, 320s, 184s, 119s, 104s

[a] In CH_2Cl_2 at room temperature. – [b] nm. – [c] $M^{-1}\cdot cm^{-1}$. – [d] $\Delta = \nu_{max}(MeCN) - \nu_{max}(hexane)$ (in cm^{-1}). – [e] In THF at room temperature.

The electronic absorption data are collected in Table 1. Due to the electron-releasing character of the $[RuCp(CO)_2]$ group, the lowest-energy absorption bands of both **1** and **2** are red-shifted compared to those of other complexes of this series such as $[Ru(SnPh_3)_2(CO)_2(i\text{-Pr–DAB})]$.[9,10] In the case of **1** this absorption band is considerably less solvatochromic than the metal-to-ligand charge transfer (MLCT) band of the structurally related complex $[Ru(Cl)(Me)(CO)_2(i\text{-Pr–DAB})]$,[6] and even less than is found for all presently known non-halide complexes of the $[Ru(L^1)(L^2)(CO)_2(i\text{-Pr–DAB})]$ series.[9,10] For **2** the solvatochromism is negligible. This is indicative of an electronic transition possessing a limited charge transfer character. Upon cooling a 2-MeTHF solution of **1** or **2** to a glassy solid at 80 K, the lowest-energy band shifts to higher energy by ca. 350 cm^{-1}.

In order to characterize the lowest-energy electronic transition, resonance Raman (rR) spectra were recorded for both complexes by irradiation into the corresponding absorption band. This technique relies on the resonance enhancement of Raman intensity for those vibrations which are coupled to the allowed electronic transition, activated by laser excitation. The wavenumbers of the observed Raman bands are collected in Table 1. The rR spectra of **1** and **2** (Figure 2) are significantly different. That of **1** shows resonantly enhanced Raman bands at 1460 cm^{-1} and 1281 cm^{-1}, which belong to ν(CN) and ν(CC) of the coordinated *i*-Pr–DAB ligand, respectively.[2] Their resonance enhancement indicates that the electronic transition involves some degree of charge transfer to the lowest π^*-orbital of the *i*-Pr–DAB ligand. Its occupation gives rise to a lengthening of the C=N bond, a shortening of the central C–C bond, and appearance of the corresponding stretching modes in the rR spectrum. The absence of a resonantly enhanced ν_s(CO) band implies that the π-back-bonding from the central Ru atom to the CO ligands is similar in the ground and excited states, which agrees with a delocalized Ru–Ru(*i*-Pr–DAB)–Sn system and a small charge transfer character of the transition. In contrast, Raman spectra obtained by excitation into predominantly MLCT transitions, for example in the case of $[Ru(Cl)(Me)(CO)_2(i\text{-Pr–DAB})]$, show a pronounced rR effect for ν_s(CO).[6] In the case of **2** the lowest-energy transition has virtually no charge-transfer character since the bands due to the internal stretching vibrations of the *i*-Pr–DAB ligand are absent in the rR spectrum. This observation is in line with the negligible solvatochromism of this absorption band. This effect of the variable charge transfer character on the resonance Raman spectrum is not a particular property of a $\sigma\rightarrow\pi^*$ transition; it has also been found for the ML(CT) transitions of $W(CO)_4(\alpha\text{-diimine})$.[11]

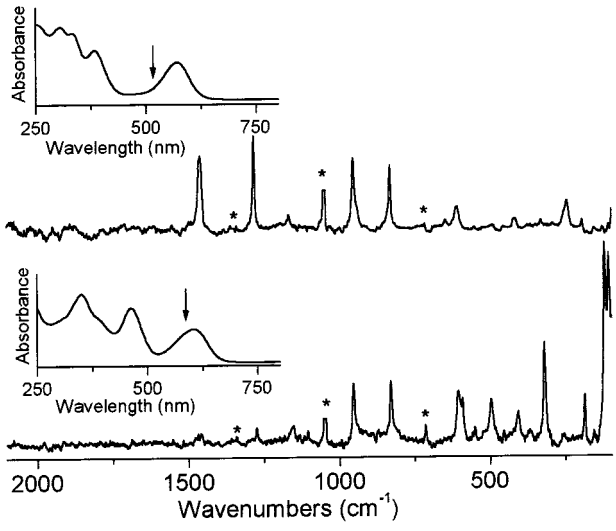

Figure 2. Resonance Raman spectra of **1** (top) and **2** (bottom) recorded by excitation (λ_{exc} = 514.5 and 590 nm, respectively) into the lowest-energy transition of the complexes dispersed in KNO_3 pellets; KNO_3 bands denoted by asterisk; UV/Vis spectra in inserts; λ_{exc} indicated by arrows

Based on the rR data, the lowest-energy absorption band of **1** is assigned to an electronic transition, qualitatively described as σ(Sn–Ru–Ru)$\rightarrow\pi^*$(*i*-Pr–DAB) with some mixing between the σ- and π^*-orbitals. In the case of **2**, this transition occurs between frontier orbitals possessing a strongly mixed σ(Ru–Ru–Ru)–π^*(*i*-Pr–DAB) character. A similar mixing between σ- and π^*-orbitals was revealed by density function calculations on the related model compound $[Ru(SnH_3)_2(CO)_2(H\text{–DAB})]$.[1] These calculations described the HOMO and LUMO as mixed contributions of a Ru p orbital, the sp^3–sp^3 combination of the SnH_3 ligands, and the π^*(H–DAB) orbital. The contribution of the π^*(*i*-Pr–DAB) orbital to the HOMO and LUMO is expected to vary from one complex to another, with a concomitant effect on the charge transfer character and the solvatochromism of the HOMO$\rightarrow$LUMO ($\sigma\rightarrow\pi^*$) transition. Going from **1** to **2**, i.e. replacing the axial $SnPh_3$-ligand by the more electron releasing $[RuCp(CO)_2]$ group, the mixing between the σ and π^* orbitals in both the HOMO and the LUMO increases. As a result the HOMO$\rightarrow$LUMO transition loses most of its charge transfer character, which is reflected in the absence of bands due to the *i*-Pr–DAB stretching vibrations

in the rR spectrum of **2**. In the 1000–100 cm^{-1} region of the rR spectrum of **1**, resonantly enhanced bands can be observed at 951 and 829 cm^{-1} (Ru–*i*-Pr–DAB metallacycle deformations) and at 609, 416, 242, and 192 cm^{-1} (metal–ligand stretching modes). These bands were also observed in the rR spectra of $[Ru(SnPh_3)_2(CO)_2(i\text{-Pr–DAB})]$ and $[Ru(SnPh_3)\{Mn(CO)_5\}(CO)_2(i\text{-Pr–DAB})]$.[2,4] In addition to these vibrations, the rR spectrum of **2** shows extra bands at 499, 320, 119 and 104 cm^{-1}, while the peak at 242 cm^{-1} is missing. The latter two bands are very intense and may belong to a ν(Ru–Ru) or a ν(Ru–Ru–Ru) mode.

Emission Properties

In a 2-MeTHF glass at 80 K, both **1** and **2** show luminescence with a much longer lifetime than that of $[Ru(Cl)(Me)(CO)_2(i\text{-Pr–DAB})]$ (Table 2).[7] This is remarkable, since **1** and **2** emit in the near infrared region, whereas the latter compound emits at much higher energy. At first, this observation seems to be in contradiction with the energy gap law. However, it can be explained by the fact that the lowest excited state has a different character. As mentioned in the introduction, the use of two σ-bound axial donor ligands results in a special type of lowest excited state. In this excited state, some electron density has been transferred from the σ-system, formed by the axial ligands and the central metal atom, to the lowest π* orbital of the α-diimine ligand, hence being called a σπ* state.[1] The long lifetime is a general property of this type of excited state, and can be rationalized as follows: In the σπ* excited state the complexes are less distorted, which is reflected in a smaller Stokes shift

Table 2. Emission properties of compounds **1** and **2** in a 2-MeTHF glass at 80 K (λ_{exc} = 532 nm).

Compound	λ_{abs} (nm)	λ_{em} (nm)	Stokes shift (cm^{-1})	τ (μs)
1	559	830	5841	16
2	593	855	5168	9
$[Ru(Cl)(Me)(CO)_2(i\text{-Pr–DAB})]$[a]	387	650	10455	0.3

[a] From ref.[7].

of their emission (Table 2). This feature originates in the delocalised nature of the electronic system, causing slight distortion of many bonds in the excited state, while the distortion along any normal coordinate is very small. Consequently, the excited state lifetime increases due to the reduction of vibrational overlap between ground and excited state wavefunctions. This situation also applies to related $[Ru(L^1)(L^2)(CO)_2(i\text{-Pr–DAB})]$ complexes, as judged from time-resolved emission and infrared data and from MO calculations.[1,2]

Photochemistry

Complexes **1** and **2** are photoreactive in solution upon irradiation into their lowest (σπ*) absorption band. The photoreactions were monitored with UV/Vis, IR, and EPR spectroscopies. The spectroscopic data of the parent complexes, photoproducts and reference compounds, are collected in Table 3 and the photoreaction pathways are summarized in Scheme 1.

First of all, solutions of **1** and **2** were irradiated in situ in an EPR spectrometer in the presence of a radical trap. The EPR spectrum recorded after irradiation of a THF solution of **1** in the presence of an excess of triphenylphosphane with a high-pressure mercury lamp ($\lambda > 455$ nm) was identical to that of the radical $[Ru(SnPh_3)(PPh_3)(CO)_2(i\text{-Pr–DAB})]^{\bullet}$, obtained by irradiation of $[Ru(SnPh_3)_2(CO)_2(i\text{-Pr–DAB})]$ in the presence of triphenylphosphane.[3] The other radical fragment, $[RuCp(CO)_2]^{\bullet}$, which was also formed by the homolysis of the Ru–Ru bond, was not observed. However, on irriadiation of **1** in toluene containing an excess of nitrosodurene, a different radical species was formed, which was identified as the nitrosodurene-trapped $[RuCp(CO)_2]^{\bullet}$ radical.[12] Exactly the same spectrum was recorded upon irradiation of **2** under the same conditions, proving that in both cases homolytic Ru–Ru bond splitting is the primary photochemical process.

In situ laser irradiation (λ_{exc} = 514.5 nm) of **1** in dichloromethane in an IR spectrometer at room temperature caused the appearance of several new bands in the CO stretching region, while those of the starting compound decreased in intensity. Initially, two bands appeared at 2056 and 2005 cm^{-1}, accompanied by three other bands at 1991, 1965 and 1936 cm^{-1}. The former two bands are assigned to $[RuCp(Cl)(CO)_2]$, in good agreement with the literature values of 2057 and 2009 cm^{-1} in CCl_4.[13] The latter three bands are attributed to $[Ru(SnPh_3)(CO)_2(i\text{-Pr–DAB})]_2$, a product which also results from photolysis of $[Ru(SnPh_3)_2(CO)_2(i\text{-Pr–DAB})]$.[3] In addition, a small peak was detected at 1773 cm^{-1}. It has been assigned to $[RuCp(CO)_2]_2$, its other ν(CO) bands being obscured by the previously mentioned bands.

On prolonged irradiation of the dichloromethane solution of **1**, new bands appeared at 2033 and 1974 cm^{-1} at the expense of the peaks belonging to $[Ru(SnPh_3)(CO)_2(i\text{-Pr–DAB})]_2$. These IR peaks and an absorption band at ca. 440 nm reveal the formation of $[Ru(Cl)(SnPh_3)(CO)_2(i\text{-Pr–DAB})]$, in agreement with literature data for this complex.[3] The dichloromethane solvent apparently does not act as an efficient radical scavenger, allowing the $[Ru(SnPh_3)(CO)_2(i\text{-Pr–DAB})]^{\bullet}$ and $[RuCp(CO)_2]^{\bullet}$ radicals to dimerise before chlorine abstraction from the solvent takes place. This applies particularly to the former radical. The photochemical quantum yield of this reaction was determined, and appeared to be rather high (0.71). These data show that σ→π* excitation of **1** causes homolysis of the Ru–Ru bond, followed by dimerisation or reaction with the solvent (Scheme 1). The Ru–Sn bond remains unaffected.

Irradiation (λ_{exc} = 514.5 nm) of **2** in spin trapping CCl_4 at 263 K gave rise to several new ν(CO) bands belonging to two chlorinated products (Scheme 1). The bands at 2058 and 2009 cm^{-1} belong to $[RuCp(Cl)(CO)_2]$, in agreement with literature data.[13] The second product [ν(CO) at 1974, 1953, 1923 and 1767 cm^{-1}] is assigned to

Table 3. Spectroscopic data of complexes **1** and **2** and their photoproducts formed upon 514.5 nm irradiation

Compound	ν(CO) (cm^{-1})	λ_{max} (nm)	solvent; temperature
1	1993m, 1961s, 1933s, 1920sh	308, 334, 384, 571	CH_2Cl_2; 293 K
$[RuCp(Cl)(CO)_2]$	2056, 2005		
$[Ru(Cl)(SnPh_3)(CO)_2(i\text{-Pr–DAB})]$	2032, 1974	≈440	
$[Ru(SnPh_3)(CO)_2(i\text{-Pr–DAB})]_2$	1991w, 1965m, 1936s		
$[RuCp(CO)_2]_2$	1773[a]		
1	1991m, 1958s, 1931s, 1915w		THF; 213 K
$[RuCp(THF)(CO)_2]^+$	2045, 1991		
$[RuCp(H)(CO)_2]$	2026, 1959		
$[Ru(SnPh_3)(CO)_2(i\text{-Pr–DAB})]_2$	1991w, 1959m, 1932s		
$[RuCp(CO)_2]_2$	1991, 1776[a]		
1	1993m, 1960s, 1933s, 1918w	308, 333, 382, 570	THF; 293 K
unassigned	2037, 2010		
$[RuCp(H)(CO)_2]$	2022, 1961		
$[Ru(SnPh_3)(CO)_2(i\text{-Pr–DAB})]_2$	1991w, 1961m, 1935s	385, 690	
$[RuCp(CO)_2]_2$	1991, 1961, 1935, 1783		
2	1996w, 1971s, 1948s, 1929s, 1922sh, 1898w		CCl_4; 263 K
$[RuCp(Cl)(CO)_2]$	2058, 2009		
$[Ru(Cl)\{RuCp(CO)_2\}(CO)_2(i\text{-Pr–DAB})]$	1974s, 1953m, 1923w, 1767w		
2	1990w, 1965s, 1945s, 1924s, 1894w		THF; 213 K
$[RuCp(THF)(CO)_2]^+$	2045, 1990		
$[Ru\{RuCp(CO)_2\}(THF)(CO)_2(i\text{-Pr–DAB})]^+$	1967s, 1943m, 1924w, 1763w		
2	1992w, 1967s, 1946s, 1926s, 1919sh, 1897w	350, 462, 604	THF; 293 K
$[RuCp(H)(CO)_2]$	2023, 1959		
$[Ru\{RuCp(CO)_2\}(THF)(CO)_2(i\text{-Pr–DAB})]^+$	1972s, 1959m, 1925w, 1764w		
$[Ru\{RuCp(CO)_2\}(CO)_2(i\text{-Pr–DAB})]_2$	1988, 1959, 1940	495, 703	
Reference compounds			
$[Ru(SnPh_3)(CO)_2(i\text{-Pr–DAB})]_2$	1988w, 1963m, 1934s	385, 690	THF[b]
$[[Ru(OTf)(SnPh_3)(CO)_2(i\text{-Pr–DAB})]$	2040, 1981		THF[b]
$[RuCp(CO)_2]_2$	2009w, 1997s, 1967m, 1955m, 1936s, 1783s	265, 331	THF
$[RuCp(CO)_2]_2$	1992s, 1965w, 1948w, 1934w, 1778s		THF; 213 K
$[RuCp(CO)_2]_2$	2002s, 1966s, 1936m, 1773s		CH_2Cl_2
$[RuCp(H)(CO)_2]$	2032, 1974		Heptane[c]
$[RuCp(H)(CO)_2]$	2022, 1960		THF
$[RuCp(H)(CO)_2]$	2025, 1953		CH_2Cl_2
$[RuCp(Cl)(CO)_2]$	2057, 2009		CCl_4[d]
$[RuCp(THF)(CO)_2]^+$	2048, 1995		THF[e]
$[Ru(Cl)(SnPh_3)(CO)_2(i\text{-Pr–DAB})]$	2033, 1974		CH_2Cl_2[f]

[a] The other ν(CO) bands are obscured by those of the other photoproducts. – [b] Ref.[3] – [c] Ref.[17] – [d] Ref.[13] – [e] With added NBu_4PF_6 electrolyte. – [f] Ref.[5]

$[Ru(Cl)\{RuCp(CO)_2\}(CO)_2(i\text{-Pr–DAB})]$. The interesting feature of this product is the ν(CO) band due to a bridging carbonyl group (1767 cm^{-1}). We assume that one carbonyl group occupies a Ru–Ru bridging position. The quantum yield of the photochemical reaction of **2** was determined to be 1.16 in CH_2Cl_2. This quantum yield, as well as that for **1** (see above), is much higher than that for $[Ru(SnPh_3)_2(CO)_2(i\text{-Pr–DAB})]$ (0.23), [3] which implies that the Ru–Ru bond is weaker than the Ru–Sn bond. A quantum efficiency higher than 1 may indicate that the radicals formed upon homolytic Ru–Ru bond splitting react with the starting compound in an electron transfer chain reaction. Similar observations were made for several related rhenium, manganese and ruthenium complexes.[14–16]

For comparison, the photochemistry of **1** and **2** was also studied in THF in the absence of radical traps (Scheme 1). In this case the major photoproduct of **1** was clearly $[Ru(SnPh_3)(CO)_2(i\text{-Pr–DAB})]_2$ [ν(CO) = 1991, 1961, 1935 cm^{-1}, λ_{max} = 385, 690 nm]. The other expected dimeric product $[RuCp(CO)_2]_2$ was only formed in a minor amount. In addition, some other bands were observed at 2037, 2022 and 2010 cm^{-1}. These peaks increased in intensity on pro-

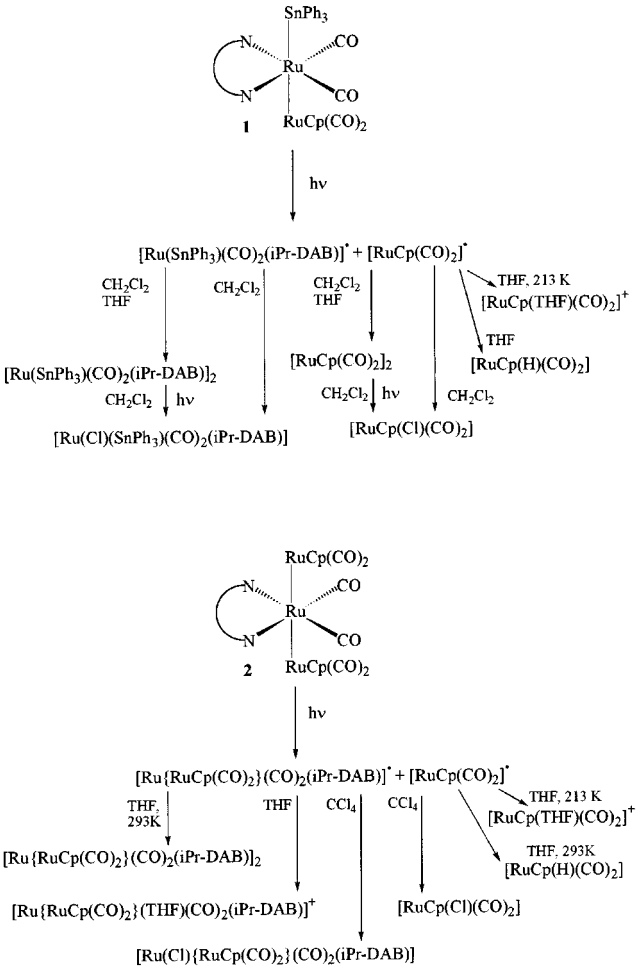

Scheme 1. Photochemical pathways of **1** and **2** in various solvents

longed irradiation, at the expense of those belonging to $[RuCp(CO)_2]_2$. The band at 2022 cm^{-1}, together with a band at 1960 cm^{-1} (hidden under the 1961 cm^{-1} band), is assigned to $[RuCp(H)(CO)_2]$, formed by the hydrogen abstraction from the solvent by $[RuCp(CO)_2]^{\bullet}$. The same ν(CO) values were found for $[RuCp(H)(CO)_2]$ synthesized from $Ru_3(CO)_{12}$ and cyclopentadiene.[17] Similar reactions of $[RuCp(CO)_2]^{\bullet}$ were reported recently.[18] The assignment of the 2037 and 2010 cm^{-1} bands is not entirely clear, but they must also belong to a species containing the $[RuCp(CO)_2]$ moiety. On irradiation at 213 K in THF the major products were the same. However, the 2037 and 2010 cm^{-1} bands were absent, whereas a new product was observed with bands at 2045 and 1991 cm^{-1}, fitting nicely with data for the $[RuCp(THF)(CO)_2]^+$ cation (Table 3).

Irradiation of a THF solution of **2** also yielded a mixture of products. Clearly visible are ν(CO) peaks at 2023 and 1960 cm^{-1} due to $[RuCp(H)(CO)_2]$. In addition, there is a series of peaks at 1967, 1943, 1924, and 1766 cm^{-1}, which probably belong to $[Ru\{RuCp(CO)_2\}(THF)(CO)_2(i\text{-Pr–DAB})]^+$, in close correspondence with the ν(CO) values for the chlorinated derivative formed in CCl_4 (vide supra). A third product with ν(CO) bands at 1988, 1960, and 1940 cm^{-1} is proposed to be $[Ru\{RuCp(CO)_2\}(CO)_2(i\text{-Pr–DAB})]_2$. This assignment is not only in agreement with the behaviour of **1**, but is also supported by the investigation of this reaction with UV/Vis spectroscopy. The product spectrum exhibits a low energy absorption band at 703 nm which is characteristic for such a dimer (Figure 3).[3] At low temperatures (213 K) no dimeric products were observed, but only the cationic species $[Ru\{RuCp(CO)_2\}(THF)(CO)_2(i\text{-Pr–DAB})]^+$ and $[RuCp(THF)(CO)_2]^+$. Apparently, the increased viscosity of the solvent at low temperatures hampers the dimerisation of the radical fragments.

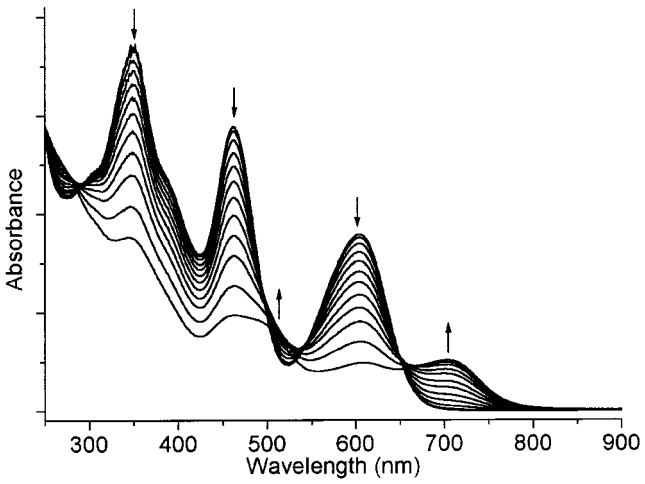

Figure 3. UV/Vis spectral changes accompanying 514.5 nm irradiation of **2** in THF at room temperature

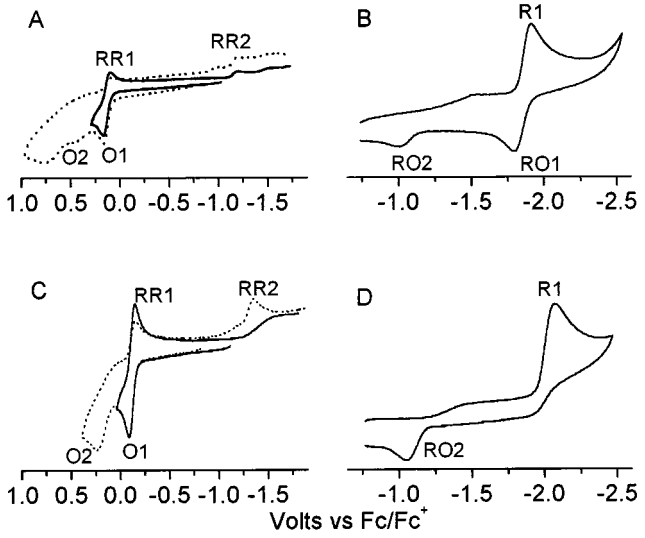

Figure 4. Cyclic voltammograms showing the oxidation of **1** (A) and **2** (C), and the reduction of **1** (B) and **2** (D) in butyronitrile solutions at 213 K

Redox Properties and Reactivity

The complexes **1** and **2** were subjected to a (spectro)electrochemical study. Cyclic voltammograms were recorded at variable temperatures to determine the electrode potentials and to study the reversibility of the corresponding redox processes (Figure 4, Table 4). The nature of the redox products was investigated by IR spectroelectrochemistry. The spectroscopic data are collected in Table 5.

Table 4. Reduction and oxidation potentials (V vs. Fc/Fc^+)

Compound	$E_{p,c}$	$E_{p,a}$	ΔE_p[a]	conditions	reference
1	–1.98	0.16		THF/293 K	this work
1	–1.89[b]	0.17	0.07	*n*-PrCN/213 K	this work
2	–2.04	0.06		THF/293 K	this work
2	–2.11	–0.09	0.06	*n*-PrCN/213 K	this work
$[Ru\{RuCp(CO)_2\}_2(CO)_2(i\text{-Pr–DAB})]^{+\bullet}$		0.24		*n*-PrCN/213 K	this work
$[RuCp(CO)_2]_2$	–2.57	0.37		THF/293 K	this work[c]
$[RuCp(THF)(CO)_2]^+$	–1.47			THF/293 K	this work[c]
$[RuCp(CO)_2]^-$		–1.27		THF/293 K	this work[c]
$[Ru(SnPh_3)_2(CO)_2(i\text{-Pr–DAB})]$	–1.91	0.34			[5]
$[Ru(SnPh_3)(CO)_2(i\text{-Pr–DAB})]^-$		–1.07		THF/293 K	[5]

[a] Anodic process, $\Delta E_p(Fc/Fc^+) = 0.06$ V. – [b] $\Delta E_p = 0.12$ V. – [c] The redox behaviour of the dimer $[RuCp(CO)_2]_2$ in THF was studied independently by cyclic voltammetry and IR spectroelectrochemistry. Literature data in ref.[31,32]

Table 5. IR spectroelectrochemical data for reduction (THF, room temperature) and oxidation (*n*-PrCN, 193 K) products of **1** and **2**

Compound	ν(CO) (cm^{-1})	conditions	reference
1	1992m, 1958s, 1930s, 1913w	*n*-PrCN/193 K	this work
1	1992m, 1969s, 1932s, 1916w	THF/293 K	this work
2	1989w, 1965s, 1946s, 1924s, 1910sh, 1897w	*n*-PrCN/193 K	this work
2	1992w, 1967s, 1946s, 1926s, 1915sh, 1893w	THF/293 K	this work
$[RuCp(n\text{-PrCN})(CO)_2]^+$	2079, 2031	*n*-PrCN/193 K	this work
$[RuCp(MeCN)(CO)_2]^+$	2090, 2044	CH_2Cl_2/293 K	[19]
$[RuCp(CO)_2]^-$	1887, 1801	THF/293 K	this work
$[Ru(SnPh_3)(n\text{-PrCN})(CO)_2(i\text{-Pr–DAB})]^+$	2041, 1987	*n*-PrCN/193 K	this work
$[Ru(SnPh_3)(OTf)(CO)_2(i\text{-Pr–DAB})]$	2040, 1981	THF/293 K	[10]
$[Ru(SnPh_3)(CO)_2(i\text{-Pr–DAB})]^-$	1924, 1856	THF/293 K	[5]
$[Ru\{RuCp(CO)_2\}_2(CO)_2(i\text{-Pr–DAB})]^{+\bullet}$	2021w, 1997s, 1981s, 1962s, 1930w	*n*-PrCN/193 K	this work
$[Ru(n\text{-Pr–CN})_2(CO)_2(i\text{-Pr–DAB})]^{2+\bullet}$	2116, 2060sh	*n*-PrCN/193 K	this work
$[Ru\{RuCp(CO)_2\}(CO)_2(i\text{-Pr–DAB})]^-$	1927, 1847	*n*-PrCN/193 K	this work

At room temperature, the oxidation of **1** is chemically completely irreversible in THF. However, at 213 K in butyronitrile two oxidation waves became apparent, with the first oxidation process (O1) being partly reversible (I_c/I_a = 0.7) on the voltammetric timescale at the scan rate of 100 mV/s (Figure 4, A). The following anodic step (O2) is completely irreversible. The fact that step O1 was found to be more than 150 mV more negatively than that of $[Ru(SnPh_3)_2(CO)_2(i\text{-Pr–DAB})]$[5] indicates that the oxidation of **1** is significantly located on the $[RuCp(CO)_2]$ moiety. Oxidising **1** at O1 led to the appearance of four bands in the IR carbonyl-stretching region. The product formation was independent of the temperature employed. The primary one-electron oxidised product detected at RR1 (Figure 4, A) at 213 K by cyclic voltammetry, is not detectable on the spectroelectrochemical timescale of seconds to minutes. Of the four bands, those at 2079 and 2031 cm^{-1} are attributed to $[RuCp(n\text{-PrCN})(CO)_2]^+$, in accordance with both the literature values of 2090 and 2044 cm^{-1} for $[RuCp(MeCN)(CO)_2]^+$ in CH_2Cl_2[19] and the observation that upon electrochemical oxidation of $[RuCp(CO)_2]_2$ in *n*-PrCN a product with identical ν(CO) wavenumbers was formed (Table 4). The two remaining bands (2042 and 1987 cm^{-1}) must be due to $[Ru(SnPh_3)(n\text{-PrCN})(CO)_2(i\text{-Pr–DAB})]^+$, as their wavenumbers are close to the values found for $[Ru(OTf)(SnPh_3)(CO)_2(i\text{-Pr–DAB})]$ (2041 and 1981 cm^{-1} in THF).[10] Taking these data into account, we propose the following oxidation path for **1**: initially, the unstable radical cation ($\mathbf{1}^{+\bullet}$) is formed, which rapidly splits to give the $[Ru(SnPh_3)(n\text{-PrCN})(CO)_2(i\text{-Pr–DAB})]^+$ cation and the $[RuCp(CO)_2]^\bullet$ radical. The latter species also binds a solvent molecule and converts to the corresponding cation in a second oxidation step. On the reverse scan, small cathodic peaks were observed (RR2, Figure 4, A), but the corresponding processes were not investigated in detail.

The oxidation of **2** is completely irreversible in THF at room temperature. However, at 213 K in butyronitrile at a v = 100 mV/s the first oxidation process (O1) is completely reversible, as indicated by ΔE_p = 61 mV and I_c/I_a = 1 (Figure 4, C). For equimolar solutions of **1** and **2** virtually the same anodic current was observed at E_a(O1) at 213 K. Considering similar values for the diffusion coefficients of **1** and **2,** this reveals that also the oxidation of **2** at low temperatures is a one-electron process. Indeed, the initial oxidation product of **2** observed in the corresponding IR-spectroelectrochemical experiment in *n*-PrCN at 193 K, exhibits a ν(CO) pattern very close to that of the parent compound **2**, but shifted by ca. 35 cm^{-1} to larger wavenumbers [ν(CO) at

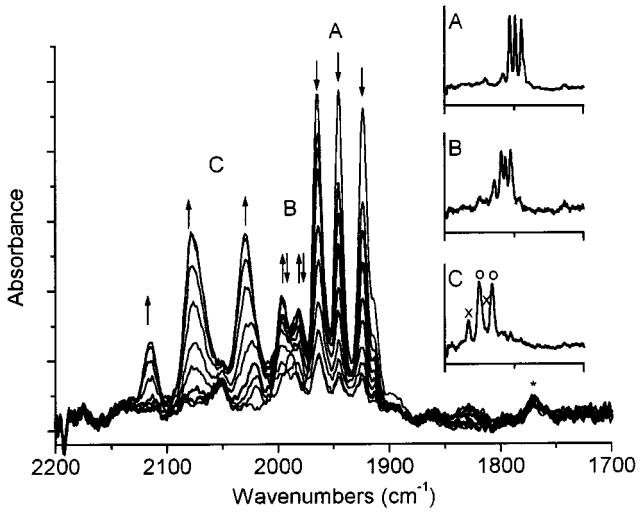

Figure 5. IR spectral changes upon oxidation of **2** in butyronitrile at 193 K. The insets are the parent compound (A), the corresponding radical cation (B), and the secondary oxidation products $[Ru(n\text{-}PrCN)_2(CO)_2(i\text{-}PrDAB)]^{2+}$ and $[RuCp(n\text{-}PrCN)(CO)_2]^+$, indicated by × and o, respectively (C). The asterisk denotes a small $[RuCp(CO)_2]_2$ impurity in the starting compound

2021, 1997, 1981, 1962 and 1930 cm^{-1}, Figure 5]. This points to a similar molecular structure of the one-electron-oxidised product compared to that of neutral **2**. We therefore concluded that at low temperatures the one-electron-oxidised product $[Ru\{RuCp(CO)_2\}_2(CO)_2(i\text{-}Pr\text{–}DAB)]^{+\bullet}$ is stable both on the voltammetric and the spectro-electrochemical time scales. This is the first time that a stable radical cation has been spectroscopically characterised for complexes $[Ru(L^1)(L^2)(CO)_2(\alpha\text{-diimine})]$, albeit at low temperatures.

The second anodic step of **2** (O2) became separated from the reversible O1 step at 213 K, but remained completely irreversible (Figure 4, C). The corresponding oxidation of $\mathbf{2}^{+\bullet}$, followed in situ by IR-spectroscopy at 193 K, produced species with ν(CO) at 2116, 2060 and 2079, 2031 cm^{-1}. The latter two bands are again attributable to $[RuCp(n\text{-}PrCN)(CO)_2]^+$, while the former two bands must be due to a highly positively charged species, e.g. $[Ru(n\text{-}PrCN)_2(CO)_2(i\text{-}Pr\text{–}DAB)]^{2+}$. The secondary oxidation products of $\mathbf{2}^{+\bullet}$ were reduced back at RR2, resulting in a mixture of the parent complex **2** and $[RuCp(CO)_2]_2$.

In THF at room temperature, the irreversible reduction of **1** at R1 (see Table 4) produced the IR-detectable anions $[Ru(SnPh_3)(CO)_2(i\text{-}Pr\text{–}DAB)]^-$ [ν(CO) at 1924 and 1855 cm^{-1}][5] and $[RuCp(CO)_2]^-$ [ν(CO) at 1887 and 1801 cm^{-1}, close to the literature data[20]]. In addition to these main bands a smaller ν(CO) peak arose at 1782 cm^{-1}. This peak can be assigned to the dimer $[RuCp(CO)_2]_2$, its remaining peaks being hidden under the other ν(CO) bands (see Table 4). The reduction path of **1** is therefore proposed to involve initially an unstable radical anion, which rapidly falls apart into the stable $[Ru(SnPh_3)(CO)_2(i\text{-}Pr\text{–}DAB]^-$ anion and the $[RuCp(CO)_2]^\bullet$ radical (see Scheme 1). The latter species partly dimerises, but the majority is reduced to the $[RuCp(CO)_2]^-$ anion at the reduction potential of **1**. The fact that the latter reduction potential is similar to that of $[Ru(SnPh_3)_2(CO)_2(i\text{-}Pr\text{–}DAB)]$[5] indicates that reduction takes place primarily on the Ru(*i*-Pr–DAB) moiety.

The radical anion $\mathbf{1}^{-\bullet}$ could only be detected by cyclic voltammetry in butyronitrile at sufficiently low temperatures (Figure 4, B). At 213 K the reduction of **1** is a chemically partly reversible one-electron process with I_a/I_c = 0.78 at v = 100 mV/s (see Figure 4, B). The final reduction products $[Ru(SnPh_3)(CO)_2(i\text{-}Pr\text{–}DAB]^-$ and $[RuCp(CO)_2]^-$ are oxidised at similar electrode potentials (Table 4). Therefore, on the reverse anodic scan the oxidation of the two anions cannot be distinguished and appears as a single anodic peak (RO2) at –1.18 V (THF, room temperature) and –1.00 V vs Fc/Fc^+ (butyronitrile, 213 K, Figure 4, B). IR spectroelectrochemistry revealed that reoxidation of both anions at room temperature at RO2 mainly regenerates the parent complex **1**. In addition, a minor amount of the dimer $[Ru(SnPh_3)(CO)_2(i\text{-}Pr\text{–}DAB]_2$ was produced at the end of the reoxidation. Obviously, $[Ru(SnPh_3)(CO)_2(i\text{-}Pr\text{–}DAB]^-$ was present in a small excess in the thin solution layer after the reduction, and therefore, once all $[RuCp(CO)_2]^-$ had been consumed in the course of the parallel reoxidation, the remaining $[Ru(SnPh_3)(CO)_2(i\text{-}Pr\text{–}DAB]^-$ was oxidised to give the dimer by a previously reported ECEC path.[5]

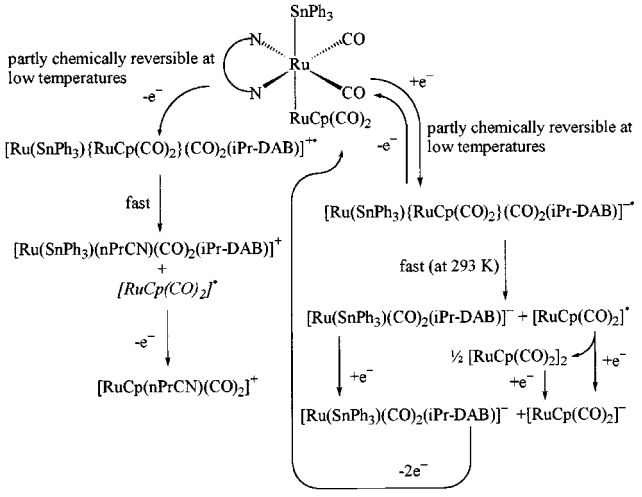

Scheme 2. Reduction and oxidation pathways of **1** in *n*-PrCN

The reduction of **2** at R1 (Figure 4, D, Table 4) is completely chemically irreversible at moderate voltammetric scan rates, independent of temperatures between 293 and 193 K. Corresponding IR spectroelectrochemical experiments again showed the formation of the $[RuCp(CO)_2]^-$ anion [ν(CO) at 1887 and 1801 cm^{-1}]. Two other ν(CO) bands observed at 1927 and 1847 cm^{-1} are tentatively ascribed to the thermally unstable $[Ru\{RuCp(CO)_2\}(CO)_2(i\text{-}Pr\text{–}DAB]^-$ anion. Attempts to prevent its decomposition by carrying out the reduction of **2** in butyronitrile at 193 K were not successful. Considering the combined voltammetric and spectroelectrochemical results, we conclude that the reduction of **2** initially yields the radical anion $[Ru\{RuCp(CO)_2\}_2(CO)_2(i\text{-}Pr\text{–}DAB)]^{-\bullet}$, which rapidly dissociates into $[Ru\{RuCp(CO)_2\}(CO)_2(i\text{-}Pr\text{–}DAB]^-$ and $[RuCp(CO)_2]^\bullet$. The latter radical further reduces to the cor-

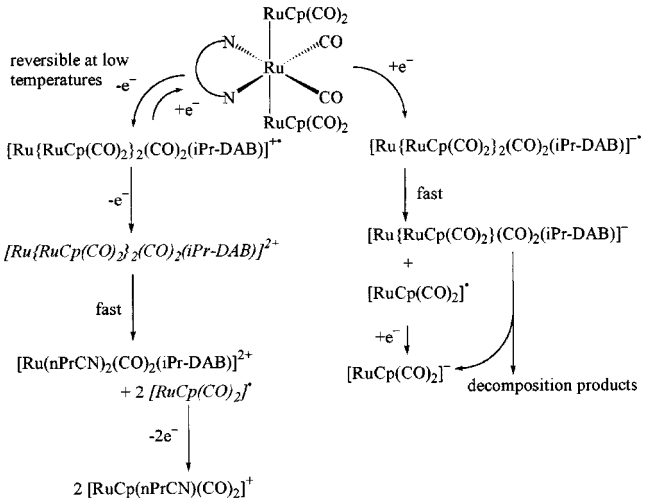

Scheme 3. Reduction and oxidation pathways of **2** in *n*-PrCN

responding anion. No dimerisation of the latter radical was observed in this case, probably due to the more negative reduction potential of **2** (see Table 4). The former anion is thermally unstable and dissociates into another equivalent of $[RuCp(CO)_2]^-$ and unidentified carbonyl products. This decomposition also explains the fact that the reverse oxidation at the anodic peak RO2 at –1.27 V (THF, room temperature) and –1.06 V vs Fc/Fc^+ (butyronitrile, 213 K, Figure 4, D) only concerns the $[RuCp(CO)_2]^-$ anion, yielding mainly the $[RuCp(CO)_2]_2$ dimer instead of recovering the parent complex **2**.

The redox behaviour of the complexes **1** (Scheme 2) and **2** (Scheme 3) differ considerably from that of the complexes $[Ru(L^1)(L^2)(CO)_2(i\text{-Pr–DAB})]$ (L^1, L^2 = $GePh_3$, $SnPh_3$, $PbPh_3$; not all combinations were investigated) previously studied in our laboratory.[5] The latter complexes are reduced reversibly, even at room temperature, producing fairly stable radical anions. In contrast, their oxidation is completely irreversible in the temperature range available. Apparently, coordination of the $SnPh_3$ axial ligands contributes significantly to the stability of the radical anion, mainly due to the strong delocalisation of the SOMO over the $(Ph_3Sn)_2Ru(i\text{-Pr–DAB})$ moiety and also due to the strong Ru–Sn bond.[1] On the other hand, the $[RuCp(CO)_2]$ units exert a stabilising influence on the radical cation, where the π-donor Cp-rings compensate for the reduced electron density on the axial ruthenium atom(s), compared to the neutral precursors. This property of Cp-rings has been recognised e.g. in the complexes $[RuCpX(i\text{-Pr–DAB})]$ (X = Cl, OTf).[21]

Concluding Remarks

The incorporation of one or two strongly donating $[RuCp(CO)_2]$ groups as axial ligands in $[Ru(L^1)(L^2)(CO)_2(i\text{-Pr–DAB})]$ yields complexes with a relatively high-lying $\sigma(L^1\text{–Ru–}L^2)$ HOMO. This is reflected in relatively negative oxidation potentials of **1** and **2** compared to other $[Ru(L^1)(L^2)(CO)_2(i\text{-Pr–DAB})]$ complexes.[1,2] As a further consequence, the emission shifts to the near infrared (NIR) spectral region, with lifetimes in the order of 10 μs at 80 K. This property is very interesting from the viewpoint of the potential use of this type of complexes as NIR emitting labels.[22–25] However, the photochemical reactivity of the studied complexes, which involves homolytic cleavage of a Ru–Ru bond as the primary photoprocess, presents a serious obstacle for such applications. The $[RuCp(CO)_2]$ group(s) also split off upon electrochemical reduction and oxidation of the complexes. The most remarkable difference between the redox behaviour of **1** and **2** and that of the previously studied $[Ru(L^1)(L^2)(CO)_2(i\text{-Pr–DAB})]$ complexes[5], is the stabilising influence of the $[RuCp(CO)_2]$ groups on the one-electron-oxidised products.

Experimental Section

General: $[Ru_3(CO)_{12}]$ (ABCR), I_2 (Merck), $SnClPh_3$ (Aldrich) and $[Ru(CO)_2Cp]_2$ (Strem) were used as received. *N,N′*-diisopropyl-1,4-diaza-1,3-butadiene (*i*-Pr–DAB),[26] $[RuCp(H)(CO)_2]$,[17] $[RuCp(CO)_2]_2$,[17] $[Ru(Cl)(SnPh_3)(CO)_2(i\text{-Pr–DAB})]$,[10] and $[Ru(I)_2(CO)_2(i\text{-Pr–DAB})]$[27] were prepared according to literature procedures. Solvents purchased from Acros (THF, 2-MeTHF, hexanes, dichloromethane) and Merck (heptane) were dried on and distilled from the appropriate drying agent. Silica gel (kieselgel 60, Merck, 70–230 mesh) for column chromatography was dried and activated by heating in vacuo at 160°C overnight. All syntheses and measurements were performed under a nitrogen atmosphere using standard Schlenk techniques. – UV/Vis: Varian Cary 4E and Hewlett-Packard 8453. – IR: Bio-Rad FTS 7 and FTS 60A, the latter equipped with a liquid nitrogen-cooled MCT detector. – NMR: Bruker AMX300 (^1H and ^{13}C) and DRX300 (^{119}Sn). – Resonance Raman: Dilor XY spectrometer, with an SP2040E Ar^+-laser as excitation source and a Wright Instruments CCD-detector. – EPR: Varian E-104A. – FAB-MS: JEOL JMS SX/SX102A four-sector mass spectrometer, coupled to a JEOL MS-MP7000 data system. Elemental analyses were performed at H. Kolbe Mikroanalytisches Laboratorium in Mülheim an der Ruhr.

Time-resolved emission spectra were recorded at 80 K in an Oxford Instruments cryostat. A Spectra Physics GCR-3 Nd:YAG laser, operating at 10 Hz was used as the excitation source. The desired wavelength (532 nm) was obtained by frequency doubling of the 1064 nm fundamental. The setup has been described elsewhere.[16]

Quantum yields of the photoreactions were determined from the disappearance of the parent complexes, following the decay of their lowest-energy absorption band. For this purpose the sample was irradiated within the UV/Vis spectrophotometer with one of the laser lines of an SP2025 Ar^+-ion laser through an optical fiber in a previously described setup.[16]

Cyclic voltammograms (CV) of approximately 10^{-3} M solutions of the parent complexes were recorded with added NBu_4PF_6 (0.1–0.3 M) as supporting electrolyte in a gas-tight, single-compartment, three-electrode cell equipped with platinum disk working (apparent surface area 0.42 mm^2), platinum gauze auxiliary and silver wire pseudoreference electrodes. The cell was connected to a computer-controlled PAR Model 283 potentiostat. Redox potentials are reported relative to $E_{1/2}(Fc/Fc^+)$ ($E_{1/2}$ = 0.575 and 0.43 V vs. SCE in THF and CH_3CN, respectively). Ferrocene was added as internal standard.[28] The scan speed was 100 mV/s. IR-spectroelectrochem-

ical measurements at variable temperatures were performed with ca. 10^{-2} M solutions in previously described optically transparent thin-layer electrochemical (OTTLE) cells.[29,30] The potential was controlled during these measurements by a PA4 (EKOM, Czech Republic) potentiostat.

[Ru(SnPh$_3$)[RuCp(CO)$_2$](CO)$_2$(*i*-Pr–DAB)] (1): [RuCp(CO)$_2$]$_2$ (215.5 mg, 0.48 mmol) was dissolved in 30 mL THF. An excess of 0.6 mL $NaK_{2.8}$ was added through a syringe under stirring. The yellow colour of the reaction mixture changed to brown yellow during the next 45 min, after which IR spectra showed virtually complete conversion into [RuCp(CO)$_2$]$^-$.[20] The resulting solution was added gradually through a syringe to a solution of [Ru(Cl)(SnPh$_3$)(CO)$_2$(*i*-Pr–DAB)] (181.7 mg, 0.24 mmol) in 30 mL THF under the exclusion of light. The reaction mixture turned purple immediately. The solvent was evaporated and the product was purified by column chromatography on activated silica, using a CH_2Cl_2/hexane eluent (1:3 v/v). The product elutes prior to the [RuCp(CO)$_2$]$_2$ main impurity. It was obtained as a purple microcrystalline solid in approximately 50% yield. – ^{1}H NMR ($CDCl_3$): δ = 0.99 {d, 6 H, ^3J = 6.5 Hz, CH(CH_3)$_2$ pointing toward SnPh$_3$, assignment based on comparison with the ^{1}H NMR spectra of [Ru(SnPh$_3$)$_2$(CO)$_2$(*i*-Pr–DAB)] (δ = 0.97)[1] and **2** (vide infra)}; 1.19 [d, 6 H, ^3J = 6.5 Hz, CH(CH_3)$_2$ pointing toward RuCp(CO)$_2$], 4.40 [sept, 2 H, ^3J = 6.6 Hz, CH(CH$_3$)$_2$], 5.22 (s, 5 H, C_5H_5), 7.27 (m, 9 H, *o*/*p*-SnC_6H_5); 7.38 (m, 6 H, *m*-SnC_6H_5); 7.87 (85% s, 15% d, 2 H, $^4J_{Sn-H}$ = 21 Hz, imine CH). – ^{13}C NMR APT (C_6D_6): δ = 25.1, 24.5 [CH(*C*H$_3$)$_2$], 63.0 [*C*H(CH$_3$)$_2$], 86.4 (C_5H_5), 128.0, 127.7 (s, *m*/*p*-SnC_6H_5), 137.8 (85% s, 15%d, J_{Sn-C} = 34 Hz, *o*-SnC_6H_5), 144.5 (s, *ipso*-SnC_6H_5), 145.4 (s, C=N), 205.7 (s, Ru$_{axial}$–CO), 209.7 (s, Ru$_{central}$–CO). – ^{119}Sn NMR ([D$_6$]acetone): δ = –45.6. – IR (THF): See Table 1. – UV/Vis: See Table 1. – FAB-MS; *m*/*z*: [M$^+$] not detected, 813 [M$^+$ – 2 CO], 764 [M$^+$ – Ph – CO], 649 [M$^+$ – RuCp(CO)$_2$].

[Ru[RuCp(CO)$_2$]$_2$(CO)$_2$(*i*-Pr–DAB)] (2): This compound was synthesized from [Ru(I)$_2$(CO)$_2$(*i*-Pr–DAB)] (103.8 mg, 0.19 mmol) following the same procedure as for **1**. It was obtained as a dark green microcrystalline solid in approximately 50% yield. – ^{1}H NMR ($CDCl_3$): δ = 1.21 [d, 12 H, ^3J = 6.6 Hz, CH(CH_3)$_2$], 4.36 [sept, 2 H, ^3J = 6.6 Hz, CH(CH$_3$)$_2$], 5.24 (s, 10 H, C_5H_5), 7.99 (s, 2 H, imine CH). – ^{13}C NMR APT (C_6D_6): δ = 24.8 [CH(*C*H$_3$)$_2$], 61.6 [*C*H(CH$_3$)$_2$], 86.4 (C_5H_5), 143.7 (C=N), 205.7 (Ru$_{axial}$–CO), 214.6 (Ru$_{central}$–CO). – IR (THF): See Table 1. UV/Vis: See Table 1. – FAB-MS; *m*/*z*: 743 [M$^+$], 521 [M$^+$ – RuCp(CO)$_2$]. – $C_{24}H_{26}N_2O_6Ru_3$ (869.52): calcd. C 38.87, H 3.53, N 3.78; found C 38.69, H 3.36, N 3.70.

[1] M. P. Aarnts, M. P. Wilms, K. Peelen, J. Fraanje, K. Goubitz, F. Hartl, D. J. Stufkens, E. J. Baerends, A. Vlček, Jr., *Inorg. Chem.* **1996,** *35*, 5468–5477.

[2] M. P. Aarnts, D. J. Stufkens, M. P. Wilms, E. J. Baerends, A. Vlček, Jr., I. P. Clark, M. W. George, J. J. Turner, *Chem. Eur. J.* **1996,** *2*, 1556–1565.

[3] M. P. Aarnts, D. J. Stufkens, A. Vlček, Jr., *Inorg. Chim. Acta* **1997,** *266*, 37–46.

[4] M. P. Aarnts, M. P. Wilms, D. J. Stufkens, E. J. Baerends, A. Vlček, Jr, *Organometallics* **1997,** *16*, 2055–2062.

[5] M. P. Aarnts, F. Hartl, K. Peelen, D. J. Stufkens, C. Amatore, J.-N. Verpeaux, *Organometallics* **1997,** *16*, 4686–4695.

[6] H. A. Nieuwenhuis, D. J. Stufkens, A. Oskam, *Inorg. Chem.* **1994,** *33*, 3212–3217.

[7] H. A. Nieuwenhuis, D. J. Stufkens, A. Vlček, Jr., *Inorg. Chem.* **1995,** *34*, 3879–3886.

[8] H. A. Nieuwenhuis, D. J. Stufkens, R. A. McNicholl, A. H. R. Al-Obaidi, C. G. Coates, S. E. J. Bell, J. J. McGarvey, J. Westwell, M. W. George, J. J. Turner, *J. Am. Chem. Soc.* **1995,** *117*, 5579–5585.

[9] M. P. Aarnts, A. Oskam, D. J. Stufkens, J. Fraanje, K. Goubitz, N. Veldman, A. L. Spek, *J. Organomet. Chem.* **1997,** *531*, 191–205.

[10] M. P. Aarnts, D. J. Stufkens, A. Oskam, J. Fraanje, K. Goubitz, *Inorg. Chim. Acta* **1997,** *256*, 93–105.

[11] R. W. Balk, D. J. Stufkens, A. Oskam, *J. Chem. Soc., Dalton Trans.* **1982**, 275–282.

[12] S. Sostero, D. Rehorek, E. Polo, O. Traverso, *Inorg. Chim. Acta* **1993,** *209*, 171–176.

[13] H. B. Abrahamson, M. C. Palazzotto, C. L. Reichel, M. S. Wrighton, *J. Am. Chem. Soc.* **1979,** *101*, 4123–4127.

[14] T. van der Graaf, R. M. J. Hofstra, P. G. M. Schilder, M. Rijkhoff, D. J. Stufkens, J. G. M. van der Linden, *Organometallics* **1991,** *10*, 3668–3679.

[15] H. A. Nieuwenhuis, M. C. E. van de Ven, D. J. Stufkens, A. Oskam, K. Goubitz, *Organometallics* **1995,** *14*, 780–788.

[16] C. J. Kleverlaan, D. J. Stufkens, I. P. Clark, M. W. George, J. J. Turner, D. M. Martino, H. van Willigen, A. Vlček, Jr., *J. Am. Chem. Soc.* **1998,** *120*, 10871–10879.

[17] A. P. Humphries, S. A. R. Knox, *J. Chem. Soc., Dalton Trans.* **1975**, 1710–1714.

[18] W. Macyk, A. Herdegen, A. Karocki, G. Stochel, Z. Stasicka, S. Sostero, O. Traverso, *J. Photochem. Photobiol. A: Chem.* **1997,** *103*, 221–226.

[19] A. Jungbauer, H. Behrens, *Z. Naturforsch. B* **1978,** *33*, 1083–1086.

[20] M. Brookhart, W. B. Studabaker, G. R. Husk, *Organometallics* **1987,** *6*, 1141–1145.

[21] B. de Klerk-Engels, F. Hartl, K. Vrieze, *Inorg. Chim. Acta* **1997,** *254*, 239–250.

[22] S. Akiyama, *Chem. Anal.* **1993,** *77*, 229–251.

[23] I. M. Warner, S. A. Soper, L. B. McGown, *Anal. Chem.* **1996,** *68*, 73R – 91R.

[24] D. C. Williams, *Anal. Chem.* **1995,** *67*, 3427–3432.

[25] G. Patonay, *Adv. Near-Infrared Meas.* **1993,** *1*, 113–138.

[26] H. Bock, H. tom Dieck, *Chem. Ber.* **1967,** *100*, 228–246.

[27] M. J. A. Kraakman, K. Vrieze, H. Kooijman, A. L. Spek, *Organometallics* **1992,** *11*, 3760–3773.

[28] G. Gritzner, J. Kůta, *Pure Appl. Chem.* **1984,** *56*, 461–466.

[29] M. Krejčík, M. Daněk, F. Hartl, *J. Electroanal. Chem. Interfacial Chem.* **1991,** *317*, 179–187.

[30] F. Hartl, H. Luyten, H. A. Nieuwenhuis, G. C. Schoemaker, *Appl. Spectroscopy* **1994,** *48*, 1522–1528.

[31] E. F. Dalton, S. Ching, R. W. Murray, *Inorg. Chem.* **1991,** *12*, 2642–2648.

[32] R. E. Dessy, P. M. Weissman, R. L. Pohl, *J. Am. Chem. Soc.* **1966,** *88*, 5117–5121.

Received September 10, 1999
[I99324]